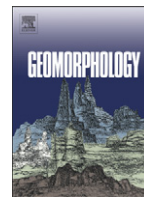




Contents lists available at ScienceDirect

Geomorphology

journal homepage: www.elsevier.com/locate/geomorph

Modeling vapor diffusion within cold and dry supraglacial tills of Antarctica: Implications for the preservation of ancient ice

Douglas E. Kowalewski^{a,*}, David R. Marchant^a, Kate M. Swanger^b, James W. Head, III^c

^a Department of Earth Sciences, Boston University, 675 Commonwealth Avenue, Boston, MA 02215, USA

^b Geology Department, Colgate University, 13 Oak Drive, Hamilton, NY 13346, USA

^c Department of Geological Sciences, Brown University, Providence, RI 02912, USA

ARTICLE INFO

Article history:

Received 18 June 2010

Received in revised form 30 October 2010

Accepted 2 November 2010

Available online 11 November 2010

Keywords:

Mullins Valley

Beacon Valley

Sublimation

Buried Ice

ABSTRACT

We modeled water–vapor diffusion within Mullins till, a relatively dry supraglacial till in southern Victoria Land, Antarctica, that rests directly on Mullins Glacier, purportedly one of the oldest alpine glaciers in the world. Like most supraglacial tills in cold-desert environments, Mullins till contains three characteristic facies: a weathered facies representing the oxidation of iron-bearing minerals and the physical disintegration of surface rocks; a sand-wedge facies representing the episodic infill of thermal cracks associated with contraction-crack polygons; and an underlying fresh facies representing the addition of englacial debris (sourced from rockfall) as overlying ice sublimates. Using a one-dimensional model for Fickian vapor diffusion through porous media, we show that the rate of subsurface ice sublimation varies by ~5.5% beneath till facies and that over timescales of 10^5 years diffusion through “porous” sand wedges contributes to the development of deep troughs surrounding high-centered polygons. Applying site-specific meteorological data collected over a four-year period, we show that ice loss at the stagnant terminus of Mullins Glacier is $\sim 6.6 \times 10^{-5} \text{ m a}^{-1}$, a value that (although low and assuming an ice thickness of ~150 m) is consistent with complete ice loss under current environmental forcing in ~2.5 Ma. Our sensitivity tests indicate that the vast majority of sublimation occurs during the summer months. Calculated summertime losses drop to zero with either a reduction in soil and ice surface temperatures of ~6.4 °C or an increase in atmospheric relative humidity from 44% to 75%, both of which could arise from an increase in cloud cover over Mullins Glacier. Sublimation responses to meteorological forcing are not uniform across Mullins Glacier. A summer increase in soil temperature of 2 °C results in negligible change in ice sublimation at Mullins terminus, but a 27% increase in ice loss in upper Mullins Valley. The key factor is the thickness of Mullins till, which is greater near the glacier terminus. For till thicknesses exceeding ~25 cm, non-linear variations in soil temperature result in downward vapor fluxes, capable of producing thin, cm-scale lenses of secondary pore that cap the surface of buried glacier ice. This downward vapor flow, sourced from modern snowfall and/or elevated atmospheric relative humidity, is one of the key factors that enable long-term preservation of buried glacier ice. Overall, our results highlight the subtle relations among changes in till texture, till thickness, and meteorological forcing on the rate of subsurface ice loss and provide insight into the plausible range of conditions under which multi-million-year-old ice can exist beneath thin supraglacial tills, <50-cm thick, in southern Victoria Land, Antarctica.

© 2010 Elsevier B.V. All rights reserved.

1. Introduction

Multiple reports suggest that stagnant glacier ice of late Miocene age exists beneath dry supraglacial tills in the Dry Valleys region of the Transantarctic Mountains, southern Victoria Land (Sugden et al., 1995; Schaefer et al., 2000; Marchant et al., 2002; Bockheim et al., 2007). If correct, the ice is considerably older than samples recovered

from even the deepest ice cores in interior East Antarctica, estimated at ~900,000 years (Augustin et al., 2004; Lambert et al., 2008). However, the age of buried ice in the Dry Valleys has been called into question on the basis of theoretical arguments that call for rapid and unsustainable ice loss via sublimation, especially as would occur in a dry, polar climate (e.g., Hindmarsh et al., 1998). These theoretical arguments rely on assumed thermomechanical properties of supraglacial tills (tills on top of buried ice) and synthetic environmental forcing; results suggest that ice losses are $\sim 1.0 \text{ mm a}^{-1}$ (Hindmarsh et al., 1998). Although very low, the value still carries with it the implication that most (if not all) buried ice deposits in the central Transantarctic Mountains are very likely < 10^5 years (Hindmarsh et al., 1998).

* Corresponding author. Current address: Climate System Research Center, Department of Geosciences, University of Massachusetts, 233 Morrill Science Center, Amherst, MA 01003, USA. Tel.: +1 413 545 1755; fax: +1 413 545 1200.

E-mail address: dkowal@geo.umass.edu (D.E. Kowalewski).

In this paper, we reexamine sublimation of buried ice deposits in the Dry Valleys. As a point of departure from earlier theoretical work, we gather site-specific field data and consider models that incorporate the effects of textural facies in supraglacial tills and measured (non-linear) temperature variations with depth (e.g., Schorghofer, 2005, 2007; Kowalewski et al., 2006). Our study focuses on Mullins till, a thin and dry supraglacial till (Bockheim et al., 2007) that rests directly on buried ice from Mullins Glacier, purportedly one of the oldest alpine glaciers in the world (Bidle et al., 2007; Marchant et al., 2007).

Our results indicate that buried ice is sublimating, but at an extremely slow rate; $<0.09 \text{ mm a}^{-1}$ near the glacier terminus. Our sensitivity tests suggest that a stable ice surface (e.g., with sublimation rates of 0.00 mm a^{-1}) is possible with only modest changes to present atmospheric conditions, e.g., consistent with an overall increase in summertime cloud cover.

2. Regional setting and background

The McMurdo Dry Valleys (MDV; 78°S latitude) occupy 4000 km^2 of predominantly ice-free terrain between the western Ross Sea and the East Antarctic polar plateau (Fig. 1). The land surface rises in a series of steps that at $\sim 100 \text{ km}$ from the coast reaches a maximum elevation of 2900 m at Mount Feather (Fig. 1). Deep, east–west trending valleys cut across the mountains and provide considerable

local relief. Given the strong covariance between summertime air temperature and bedrock elevation in the MDV (Doran et al., 2002), environmental conditions vary widely but predictably (Marchant and Denton, 1996). On the basis of measured changes in summertime atmospheric temperature, relative humidity, soil temperature, and soil moisture, Marchant and Head (2007) divided the region into three microclimate zones, each fostering a unique suite of endemic landforms: a coastal thaw zone, an inland-mixed zone, and a stable upland zone. Mullins Glacier lies within the stable upland zone (Fig. 1), a region with extremely cold atmospheric temperatures (mean summertime temperature $\sim -11^\circ\text{C}$ and mean annual temperature of -23°C) and dry conditions (Doran et al., 2002; Kowalewski et al., 2006; Vieira et al., 2010). Such conditions ensure that ablation is entirely via sublimation, with no observable melt at the surface of buried glacier ice.

2.1. Mullins Glacier

Mullins Glacier is a small, debris-covered alpine glacier that descends from bedrock slopes incised in Ferrar dolerite, Beacon Heights orthoquartzite, and Arena sandstone at the head of Mullins Valley (77.874°S , 160.537°E) (Fig. 2). It is $\sim 8 \text{ km}$ long, between 0.5 and 0.7 km wide, and up to $\sim 150 \text{ m}$ at its thickest measured point (Shean et al., 2007; Shean and Marchant, 2010). It is sourced from a

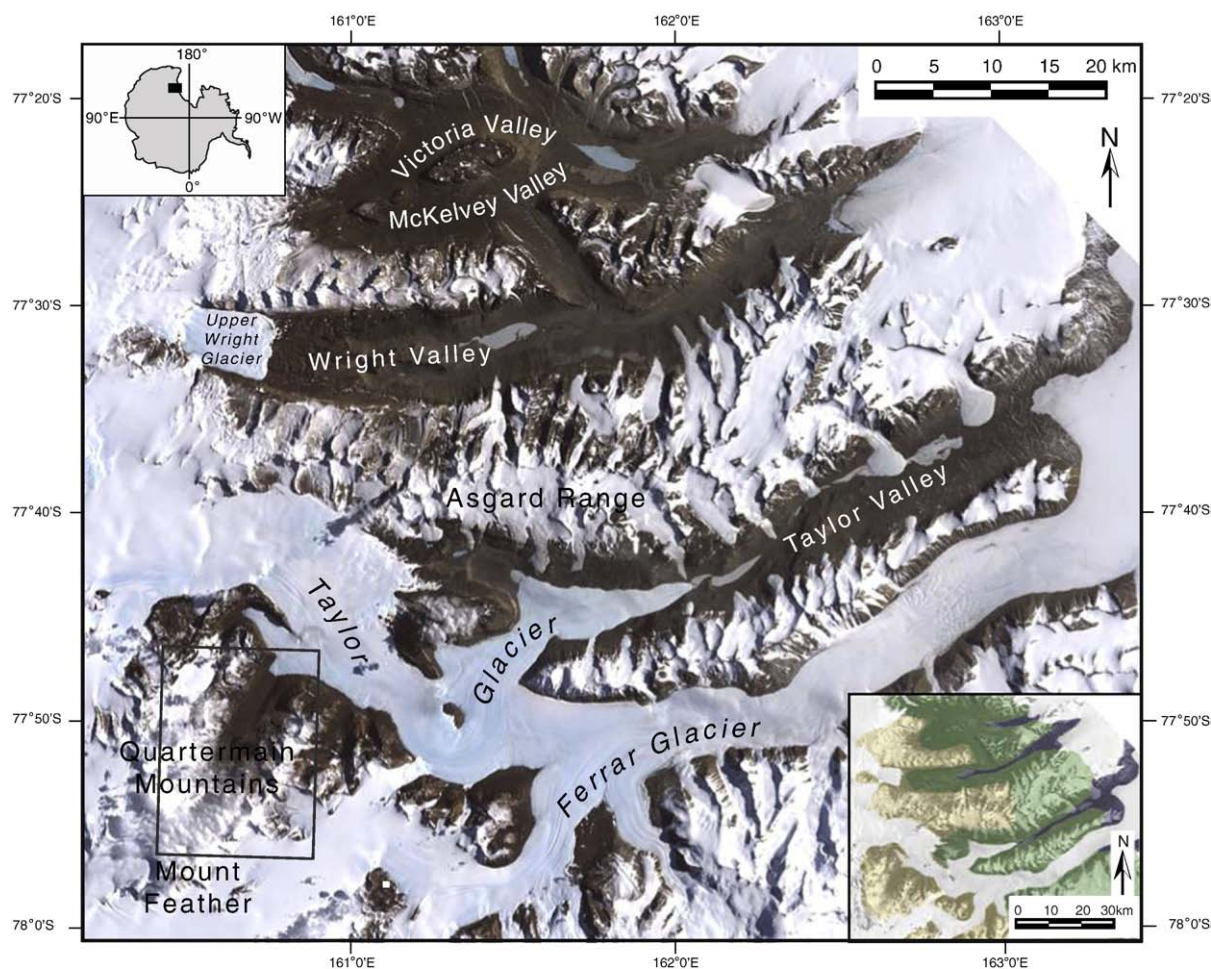


Fig. 1. Satellite image of the McMurdo Dry Valleys. Centered at $\sim 77^\circ 35' \text{S}$, the region encompasses $\sim 4000 \text{ km}^2$ of predominantly ice-free terrain between the western Ross Sea (off image to the right) and the East Antarctic polar plateau (off image to the left); top left inset shows location of the MDV on the sketch of the Antarctic continent. Lower right inset shows geomorphic zones for the MDV as defined by Marchant and Denton (1996) and Marchant and Head (2007); dark blue is the coastal thaw zone (CTZ); green is the inland-mixed zone (IMZ); and tan is the stable upland zone (SUZ) (see text for details). The box in the Quartermain Mountains, SUZ, outlines Beacon Valley and merging tributaries, including the Mullins Valley tributary (see Fig. 2 for details).

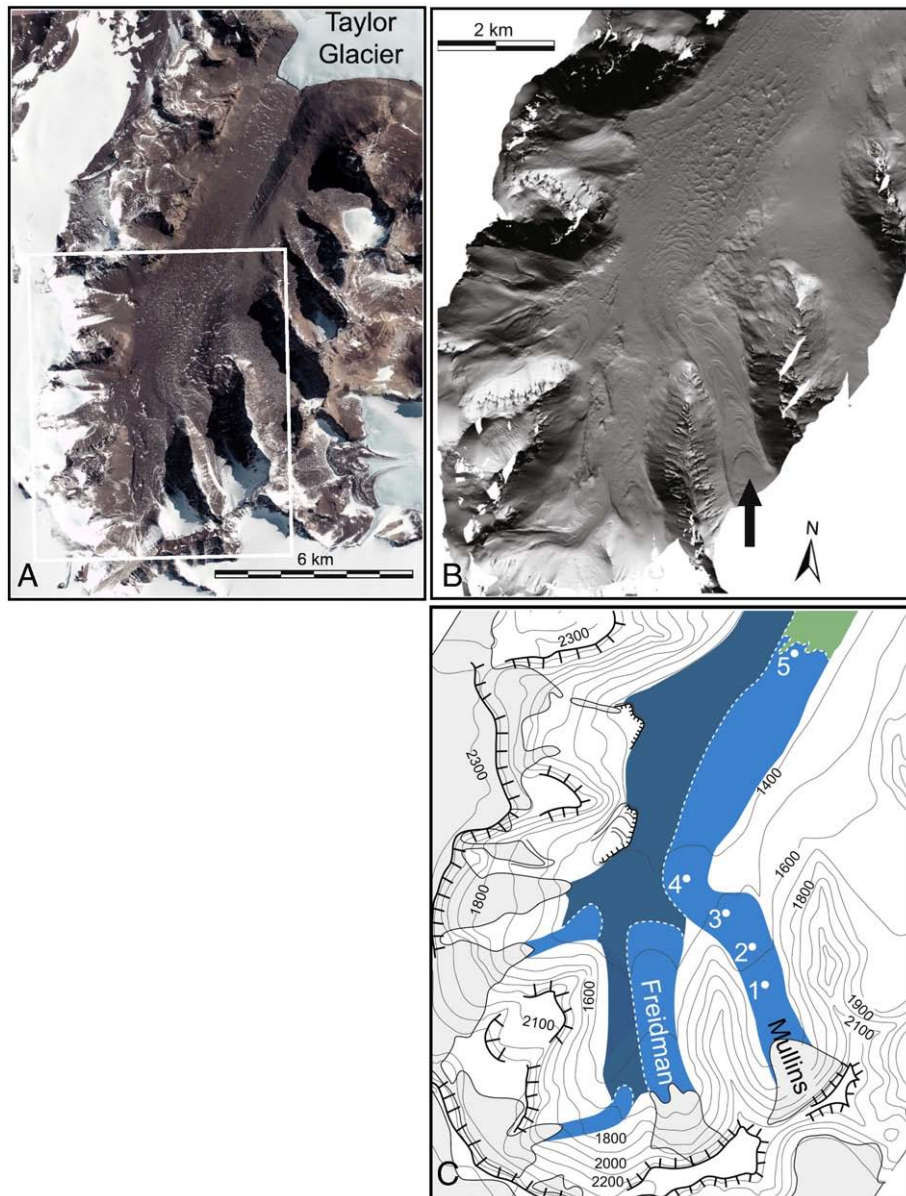


Fig. 2. (A) Landsat image showing Beacon Valley and merging tributary valleys. White box highlights region depicted in (B) and (C). (B) Hillshade image of Mullins Valley (arrowed) and surrounding region generated from high resolution airborne LiDAR digital elevation model (DEM) [collected as a joint effort by the U.S. National Science Foundation (NSF)/NASA/U.S. Geological Survey (USGS) with processing by T. Schenk and others (http://usarc.usgs.gov/lidar/lidar_pdfs/site_reports_v5.pdf)] embedded in 30-m DEM of the entire Dry Valleys region derived from stereo Corona satellite imagery (available from USGS Antarctic Resource Center). (C) Topographic map for region covered in (B). Light blue color highlights locations where debris-covered glacier ice is sourced from extant alpine glaciers; dark blue depicts regions where glacier ice is ≥ 1 m below the surface; green represents the southernmost extent of the buried ice associated with an ancestral advance of Taylor Glacier up into central Beacon Valley (e.g., Sugden et al., 1995); see text for details.

small ice accumulation zone between ~ 2200 and ~ 1700 m elevation and terminates at ~ 1270 m elevation in central Beacon Valley.

Mullins Glacier is slow moving to stagnant. Based on synthetic aperture radar interferometry, Rignot et al. (2002) showed that the modern horizontal ice flow velocity of Mullins Glacier slows from a maximum of $\sim 40 \text{ mm a}^{-1}$ near the valley head to $< 1 \text{ mm a}^{-1}$ (essentially stagnant with measurement error) where it abuts relict glacier ice from Taylor Glacier in central Beacon Valley (Sugden et al., 1995; see also below and Fig. 2).

Several debris-covered glaciers converge in central Beacon Valley (Fig. 2). Mapping their areal extent is challenging, as neither moraines nor obvious morphologic features mark contacts. Rather, differentiation is made possible only on the basis of mapping lithological characteristics of englacial and supraglacial debris. Mullins till, as well as debris in underlying Mullins glacier ice, is composed of local rock

units that crop out at the valley headwall (Shean and Marchant, 2010); whereas relict ice from Taylor Glacier and its capping supraglacial till, granite drift, contain granite and metamorphic erratics from outside Beacon Valley (Sugden et al., 1995; Marchant et al., 2002). Unlike Mullins Glacier, Taylor Glacier advanced southward up into central Beacon Valley (Fig. 2).

2.2. Mullins till, contraction-crack polygons, and facies evolution

Given its slow-moving to stagnant ice flow velocity, low ice temperatures, and limited ice thicknesses, Mullins Glacier is almost certainly cold based (a frozen ice condition in which basal ice temperatures lie below the pressure melting point). Simple one-dimensional thermal models that assume negligible strain heating (and are tuned to measured borehole temperatures of -22.4 °C at

10 m depth and -21.5°C at 30 m depth), suggest that basal ice in central Beacon Valley approaches -16.1°C . Such frozen ice conditions suggest that basal regelation is unlikely and that debris entrained in Mullins Glacier most probably originates from rockfall events at the valley headwall. Rocks that come to rest on the ice accumulation zone are likely buried beneath subsequent snow and ice, facilitating englacial transport before ultimately returning to the ice surface as overlying ice sublimates; rocks that fall onto the ice ablation zone, however, travel exclusively as supraglacial debris. The percentage of Mullins till that has been transported solely as supraglacial debris, or that has included a component of englacial flow, is unknown. However, the ratio has likely varied over time as a function of changes in the rate of rockfall and snow accumulation, as well changes in the size and geometry of the ice accumulation zone and nearby bedrock slopes (e.g., Ackert, 1998). Detailed field mapping suggests that rockfall sources for Mullins till are restricted to the headwall. Colluvial sheets and talus cones that occur along the walls of Mullins Valley do not extend out onto the glacier surface. Instead, a near-continuous linear depression, up to 3 m deep, separates the lateral margins of Mullins Glacier from adjacent colluvium/talus on valley sidewalls.

The surface of Mullins till is dominated by contraction-crack polygons (Levy et al., 2006; see also Linkletter et al., 1973; Bockheim et al., 2009) (Fig. 3). In general, polygon shape and size vary predictably downglacier (Levy et al., 2006), with the largest polygons occurring several kilometers from the headwall, in the region of inferred ice stagnation in central Beacon Valley (the largest of these polygons are ~ 20 m across; Fig. 3).

As noted in Marchant et al. (2002), supraglacial tills in hyperarid, cold climates develop three characteristic facies: a near-surface weathered facies representing oxidation of iron-bearing minerals and physical disintegration of surface rocks; a sand-wedge facies representing episodic infill of thermal contraction cracks at polygon margins; and an underlying fresh facies, representing the direct contribution of englacial debris (typically sourced as fresh rockfall) as overlying ice sublimates. All three facies are observed in Mullins till.

In places, one or more of the facies may be cemented by pore ice, e.g., secondary ice formed as water vapor moves down into the till and refreezes at depth (Marchant et al., 2002). The pore ice is likely related to snowfall, with meltwater along the margins of solar-heated rocks creating elevated soil moisture and vapor (Kowalewski et al., 2006; McKay, 2009). Given appropriate soil temperature conditions and till

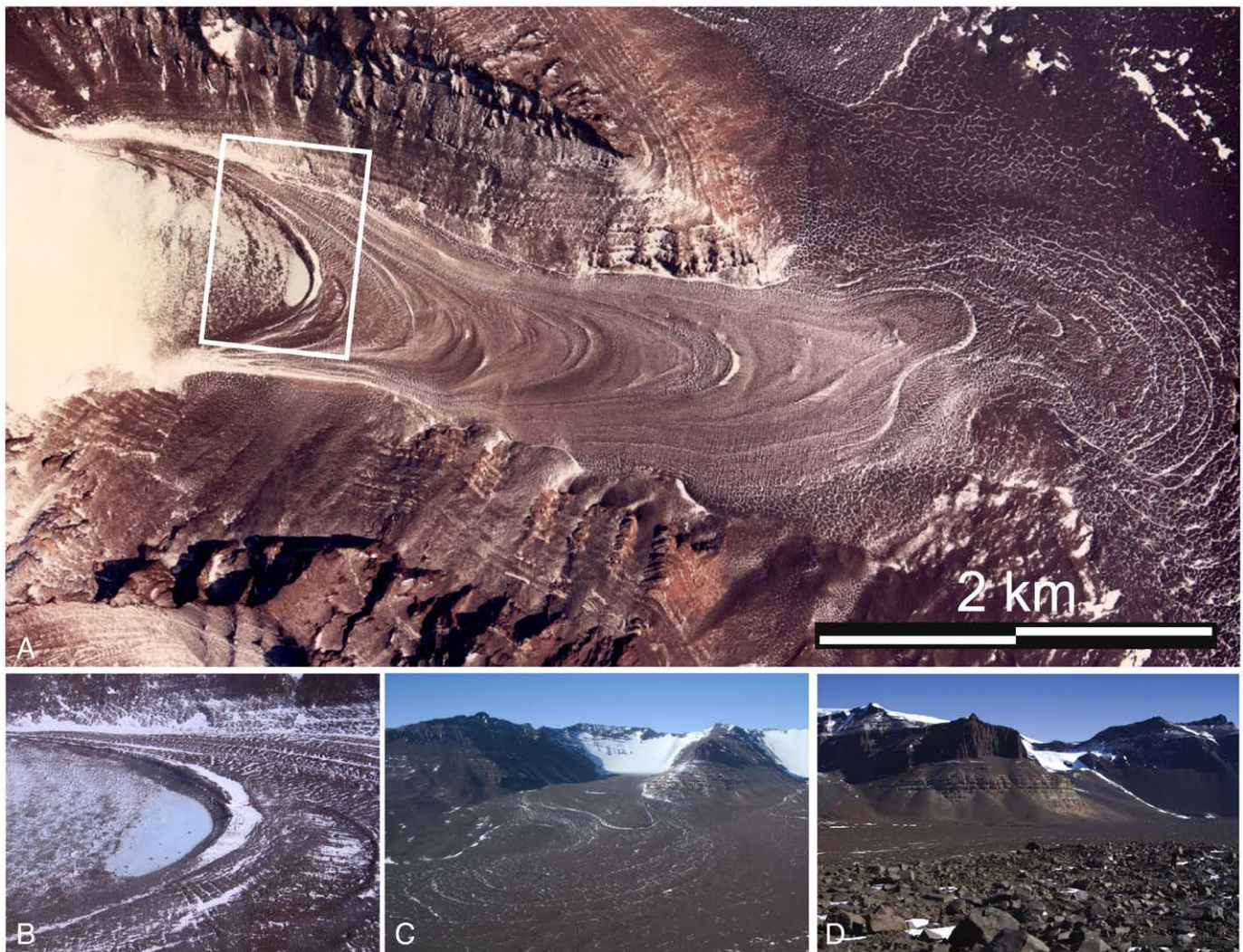


Fig. 3. (A) Vertical aerial photograph of the upper portion of the Mullins Glacier (image from USGS aerial photograph, TMA 3080). (B) Oblique-areal view of upper Mullins Glacier showing abrupt transition from scattered surface rocks to uniform debris cover (Mullins till); the transition occurs at the first of several transverse ridges to cross Mullins Glacier; location plotted as white box in (A) (see also Shean and Marchant, 2010). (C) Oblique aerial view looking SE up into Mullins Valley, as viewed from the west wall of upper Beacon Valley. The ice accumulation zone (far background) lies between ~ 2200 and 1700 m elevation; bedrock exposures at the valley headwall consists primarily of Ferrar dolerite and Beacon Heights orthoquartzite. (D) Surface of Mullins till in central Beacon Valley; the largest dolerite boulder in foreground is ~ 75 cm wide.

thicknesses, vapor may move deep into the ground (see below) and refreeze atop the buried ice surface, producing visible pore ice (Marchant et al., 2002; Kowalewski et al., 2006). These secondary ice lenses contrast markedly with glacial ice by lying on a δD versus $\delta^{18}O$ slope of 5 rather than a precipitation slope of 8 and by possessing a strongly negative deuterium excess (Marchant et al., 2002).

3. Methods

Our numerical models for vapor diffusion through Mullins till require quantitative input regarding the thickness, texture (grain size and porosity), and thermal properties of Mullins till (specific to each facies), as well as the local meteorological forcing that drives vapor diffusion.

3.1. Thickness, texture and thermomechanical properties of Mullins till

Thickness data for Mullins till come from field measurements of over 250 soil excavations. Till thicknesses are based on the measured depth of the matrix fraction (± 1 cm) and do not include the height of surface cobbles and/or boulders that cap Mullins till (Fig. 3D). All measures for till thickness come from polygon centers, not from polygon margins where local thinning and thickening from minor mass wasting into polygon troughs obscures general trends in till thickness (Marchant et al., 2002; Levy et al., 2006).

Grain size data for each facies come from analyses of the <16-mm fraction using standard wet and dry sieving techniques (>50 samples, each ~2 kg, from 42 different soil excavations). To determine minimum porosity values for each facies, we collected *in situ* sediment samples from the finest grain size fraction observed in the field by inserting the leading edge of a 10-cm wide by 8-cm deep by 20-cm long aluminum C-channel into exposed soil sections. Areas with highest gravel content were avoided during sampling. Once removed, we wrapped the samples and aluminum casing with plaster of paris to prevent movement. At Boston University, we placed the samples in a bath of styrene monomer polyester resin, resulting in uniform impregnation and cementation through gravity and capillary action alone. The impregnated casts were allowed to harden in a drying oven at 70 °C for five days and then cut into thin sections for image

analyses. We calculated pore size in two dimensions via MATLAB image analysis. Measures for the degree of soil development are based in part on visible staining (rubification) as gauged in the field by reference to standard Munsell color equivalents (MCE).

3.2. Meteorological data collection

To understand better the range of meteorological conditions in the study region, we installed a network of 10 micrometeorological stations (HOBO™ Smart Sensor weather probes, Onset Computer Corporation) at five locations (Fig. 2; Tables 1a, 1b, 1c) and collected data from December 2003 to December 2009. A detailed subset of meteorological data was collected from 3 to 24 December 2006. As noted in Tables 1a, 1b, 1c each meteorological station housed sensors for measuring a combination of solar radiance, relative humidity, atmospheric temperature, soil temperature, and soil moisture. Precise sensor placement depended on site-specific characteristics. However, in most cases soil temperature sensors were placed at the ground surface and at subsequent 10-cm depth increments; atmospheric temperature sensors were located 10 cm above the ground surface, with sensors housed in white PVC radiation shields supplied by Onset Computer Corporation (Tables 1a, 1b, 1c); soil moisture sensors were placed ~2 cm below the ground surface (and at two localities on the buried ice surface itself). Wind speed and wind direction were collected at a single locality halfway down Mullins Glacier (Fig. 2; Tables 1a, 1b, 1c); data collection for all sensors occurred at 15-min intervals. Our measured changes in soil temperature with depth enabled calculation of soil thermal diffusivities for each facies as described in Section 5.1 below.

4. Results

4.1. Variations in the thickness of Mullins till

The thickness of Mullins till increases downvalley, varying inversely with modern horizontal ice flow velocity (Fig. 4). In the region of relatively fast ice flow near the valley head, Mullins till is composed of scattered dolerite grus, rock fragments, and isolated cobbles; the debris covers <10% of the local glacier surface. At ~1300 m from the headwall,

Table 1a
Summer climate data from Mullins Valley, 3–24 December 2006.

Meteorological station	Elevation (m)	Distance down valley (km)	Depth to ice (cm)	Furthest penetration of 0°C isotherm (cm) ^a		Temperature (°C)					Atmospheric RH (%)			Solar radiance (W/m ²)		
						Mean	Min	Max	Diurnal variation (average)	Diurnal variation (max)	Mean	Min	Max	Mean	Min	Max
Site 1	1550	2.5	10	4.2	Atmosphere	-11.7	-18.1	-2.9	7.9	11.7	51.7	15.3	86.3	242.7	16.9	943.1
					Till surface	-7.6	-18.0	7.8	16.3	25.7						
					Till / ice contact (10 cm)	-10.6	-13.8	-6.9	3.7	5.7						
Site 2	1524	3.0	15	5.9	Atmosphere	-10.6	-18.1	-2.4	8.7	12.5	48.8	13.3	86.8	270.3	16.9	854.4
					Till surface	-8.2	-17.8	10.9	18.4	28.3						
					Till / ice contact (18 cm)	-12.1	-13.8	-11.0	0.7	1.3						
Site 3	1442	3.8	22	14.6	Atmosphere	-10.4	-16.7	-3.4	6.0	9.2	47.6	13.8	87.3	273.8	16.9	751.9
					Till surface	-4.5	-14.5	14.1	16.0	26.1						
					Till / ice contact (22 cm)	-7.9	-10.4	-5.0	2.3	3.5						
Site 4	1374	4.5	25	12.1	Atmosphere	-8.8	-14.7	-1.1	6.7	9.5	42.2	7.8	86.3	-	-	-
					Till surface	-2.8	-11.9	11.9	13.1	19.7						
					Till / ice contact (25 cm)	-9.7	-11.0	-8.3	0.6	0.8						
Site 5	1272	7.8	50	10.0	Atmosphere	-8.4	-13.5	-0.6	6.4	9.0	44.0	8.8	86.8	306.8	55.6	890.6
					Till surface	-3.8	-12.6	11.5	15.6	22.2						
					Till / ice contact (50 cm)	-11.8	-13.1	-11.1	0.2	0.5						

Atmospheric temperatures taken 10 cm above the till surface.

^a Furthest penetration of 0 °C isotherm was calculated using a linear interpolation between measured soil temperatures.

Table 1b
Climate data from Mullins Valley, 3 December 2006–2 November 2008.

Meteorological station	Elevation (m)	Distance down valley (km)	Atm T mean (°C)	Atm T min (°C)	Atm T max (°C)	Diurnal variation (max, cm)	Furthest penetration of 0 °C isotherm (cm)	RH mean (%)	RH min (%)	RH max (%)	SR mean (W/m ²)	SR min (W/m ²)	SR max (W/m ²)
Site 2	1524	3.0	−23.4	−45.5	1.6	17.0	7.6	59.8	8.3	92.8	NA	0.6	936.9
Site 4	1374	4.5	−21.7	−45.4	4.6	21.3	16.6	50.4	5.3	91.8	NA	0.6	799.4
Site 5	1272	8.6	−23.3	−50.5	5.0	22.5	19.1	47.8	4.3	91.8	NA	0.6	890.6

Atmospheric temperatures taken at 10 cm above till surface. Long-term meteorological data were not collected at Site 1 and Site 3.

Table 1c
Climate data from Mullins Valley, 3 December 2004–3 December 2009.

Meteorological station	Elevation (m)	Distance down valley (km)	Atm T mean (°C)	Atm T min (°C)	Atm T max (°C)	Diurnal variation (max, cm)	Furthest penetration of 0 °C isotherm (cm)	RH mean (%)	RH min (%)	RH max (%)	SR mean (W/m ²)	SR min (W/m ²)	SR max (W/m ²)
Site 5	1272	8.6	−23.4	−50.5	5.0	22.5	19.1	49.2	4.3	93.3	NA	0.6	890.6

Atmospheric temperatures taken at 10 cm above till surface. Five year meteorological dataset is not available for Sites 1–4.

the till grades from isolated cobbles, fragments, and grus to a uniform sheet, ~10–15 cm thick, that mantles the entire ice surface (Fig. 3). The transition is abrupt and occurs at the leading edge of the first of several transverse ridges that mark the glacier surface (Fig. 3 and caption; Shean and Marchant, 2010). For the next ~2 km, Mullins till maintains a steady average thickness of 15–20 cm, even where it passes across subsequent topographic ridges; the latter observation indicates that ridge relief (from 1 to 8 m) arises from changes in the level of underlying glacier ice rather than from local thickening of Mullins till (see also Shean and

Marchant, 2010; Fig. 4). At ~3.5 km from the valley headwall, where ice flow velocities slow, Mullins till thickens progressively to ~40 cm. On the floor of central Beacon Valley (≥5 km from the headwall and where horizontal velocity is <1 mm a^{−1}), Mullins till reaches its average maximum thickness between ~50 and ~70 cm (Fig. 4).

4.2. Facies within Mullins till

4.2.1. Weathered facies: near-surface physical disintegration and minor chemical alteration

The weathered facies of Mullins till averages 15–20 cm in thickness and shows marked reddening from oxidation of iron-bearing minerals (rubification; from 10YR 5/4 in upper Mullins Valley to 5YR 5/7 in central Beacon Valley). Its maximum depth of ~20 cm is uniform across the glacier and corresponds with the deepest recorded penetration of the 0 °C soil isotherm (Table 1b). The weathered facies is composed of sand- to gravel-sized fragments of Ferrar dolerite (≥96%) (mostly grus) and undifferentiated sandstone (≤4%); in most places, grus, rock fragments, and isolated mineral grains (especially pyroxene) are demonstrably related to the physical disintegration of weathered cobbles and boulders of Ferrar dolerite at the ground surface (e.g., Bockheim, 2010).

4.2.2. Fresh facies: direct sublimation of glacier ice with rockfall debris

The fresh facies underlies the weathered facies in about 30% of our soil excavations. It is distinguished in the field as an abrupt change in color and texture and, typically, appears as a gray (2.5Y 7/2) admixture of sand- to gravel-sized clasts of Ferrar dolerite (≥93%); undifferentiated sandstone (≤6%); and a matrix of quartz-rich sands, green and maroon siltstone (<2 mm in length), and abundant dolerite rock fragments. The contact with overlying weathered facies is sharp and occurs over a vertical distance of <2 cm.

All clasts within the fresh facies lack evidence for chemical alteration and long-term exposure at the ground surface (e.g., no stains, varnish, pits, or wind-related facets and scours on clasts; Marchant and Head, 2007). Instead, clasts exhibit fresh-appearing surfaces with chipped corners and isolated gouges (Fig. 5). The chipped corners and gouges are typically fringed with loose rock powder, suggestive of formation by high energy, grain-to-grain impacts as might occur during rockfall events at the valley headwall (in fact, striking one dolerite clast against another produces identical marks). The rock powder on clasts within the fresh facies is typically <0.1 mm thick and easily removed with water. The latter attests to the very dry conditions of Mullins till at depths below 20 cm (the maximum depth of the weathered facies).

The fresh facies readily collapses on exposed soil pit walls. This mechanical instability likely arises as initially dispersed englacial

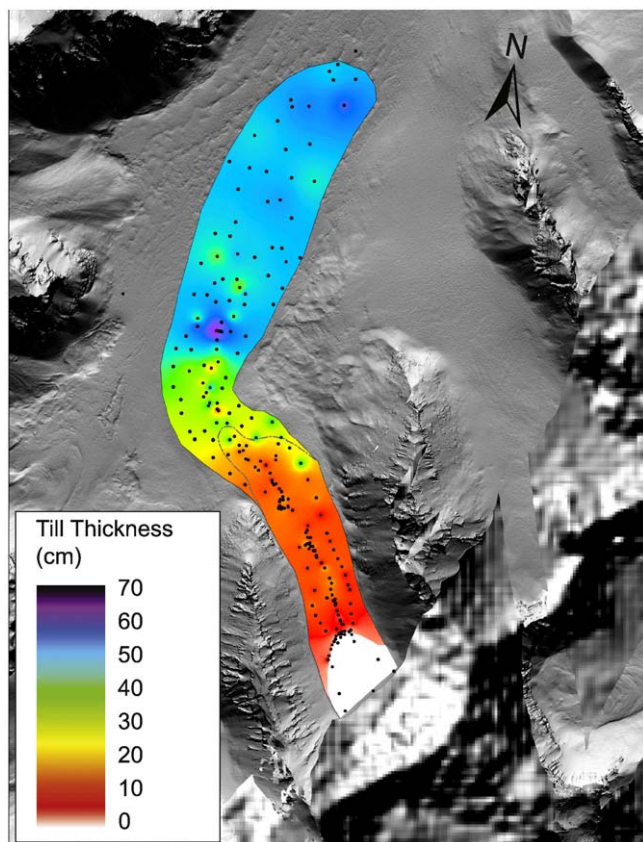


Fig. 4. Plot showing variation in the thickness of Mullins till as a function of increasing distance downglacier. The colors represent a geographic information system (GIS) interpolation of direct thickness values as measured from soil excavations in the field (black dots, *n* = 258, see text); thickness data are draped on the hillshade image shown in Fig. 2B; the lower quality resolution in lower right corner reflects splice with 30-m DEM (see also Shean and Marchant, 2010).



Fig. 5. Textural characteristics of facies within Mullins till. (A) A fresh (unweathered) clast (dolerite) removed from the fresh facies of Mullins till; the color variation reflects locations of impact gouges and loose powder coating the clast that likely formed during initial rockfall deposition. (B) A close up view of gouges fringed with loose powder on a separate clast removed from the fresh facies; all clasts within the fresh facies lack evidence for surface weathering features/chemical alteration. (C) A section of Mullins till exposing the weathered facies (upper 15 cm) and underlying fresh facies; note that clasts at the surface are coated with rock varnish and lack evidence for impact gouges. (D) Detail of the base of soil excavation in (C); the buried ice surface (gray color) lies at a 60-cm depth and is smooth and dry, without evidence for melting and/or the formation of superposed, secondary ice. Fresh-appearing dolerite clasts are partly embedded in the glacier ice; upon removal, these embedded clasts are shown to contain impact scars on all sides, such as those seen in (A) and (B). (E) A ~1-m³ boulder within Mullins till, the upper 15 cm of which reveals the effect of surface and near-surface weathering; below 15-cm, the dolerite boulder appears fresh and without visible evidence for chemical alteration. A relict sand-wedge deposit occurs to the left of the boulder, whereas a small portion of the fresh facies capped by the weathered facies occurs to the right.

clasts are brought together via sublimation of intervening ice (e.g., Lewis et al., 2007). Ultimately, the clasts are stacked precariously at the buried ice surface, each with minimal grain contacts, and hence fall readily from the surface of exposed soil pit walls. Paired analyses of englacial clasts and exposures of the fresh facies located immediately above show identical characteristics in terms of grain size distribution, grain shape, lithology, and surface textures, including chipped corners, gouges, and fringing powder.

4.2.3. Sand-wedge facies: periodic infilling of thermal contraction cracks

The sand-wedge facies forms as aeolian and/or slumped debris periodically fills open thermal contraction cracks at polygon margins (e.g., Pewe, 1959; Marchant et al., 2002; Levy et al., 2006). Repeated infilling produces a downward-tapering wedge of stratified sand and gravel that may penetrate several meters down into glacier ice. In cross section, the sand wedges display an overall trend toward coarser grains at the top and center. Relict wedges, e.g., those wedges no longer associated with active thermal contraction crack polygons (Berg and Black, 1966), also occur within Mullins till. Typically, these

wedges are deformed, being contorted in accordion-like fashion as buttressing ice is lost via sublimation. Indeed, as thermal cracks shift, initially upright wedges grade sequentially into subvertical to subhorizontal lenses (Marchant et al., 2002) (Fig. 6). The evolving stratigraphy is complex, as sand-wedge deposits truncate all facies of Mullins till, even other sand wedges (Fig. 6).

4.3. Porosity variation

Because porosity is a key factor that regulates vapor diffusion through supraglacial tills (see Section 5.1), we measured the rate-limiting porosity for each facies (e.g., the porosity of the finest grain size fraction observed in the field). Thin-section analyses (Fig. 6) show that the porosity averages 29%, 29.5%, and 31% for the weathered, fresh, and sand-wedge facies, respectively (Table 2). As noted below, these small variations in porosity appear sufficient to impact ice sublimation and long-term landscape evolution over buried glacier ice (Section 5.2).

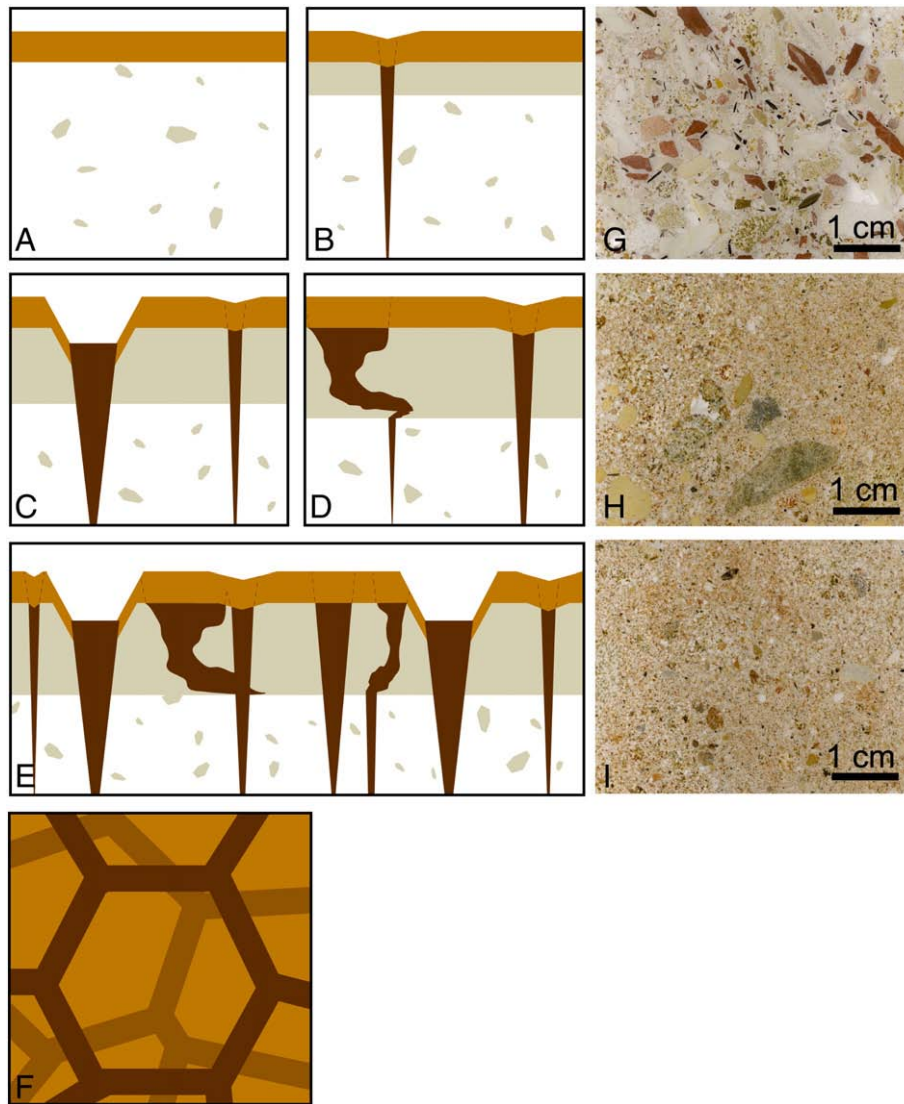


Fig. 6. Conceptual diagram showing the development and subsequent modification of all three facies of Mullins till. In (A), a 15-cm-thick weathered facies (brown) rests directly on buried glacier ice; the fresh facies is not present as the entire thickness of Mullins till lies within the zone of near-surface weathering (this is the case for most of upper and central Mullins Valley). In (B), continued sublimation of ice with pristine rockfall debris produces a fresh facies of Mullins till (tan) that lies below the weathered facies; note physical lowering of the buried ice surface from (A) to (B); also, a thermal contraction crack filled with stratified sands and gravels (dark brown) truncates both facies. In (C), continued growth of the sand wedge initiated in (B), as well as the development of a new wedge, increases the overall proportion of the sand-wedge facies in Mullins till; the mature sand wedge is now associated with a deep polygon trough (see text for explanation; Marchant et al., 2002). In (D), thermal contraction is abandoned at the first sand-wedge site (e.g., Berg and Black, 1966; Marchant et al., 2002; Levy et al., 2006); and as the ice surface continues to lower via sublimation, the once near-vertical sand wedge tilts to one side (in accordion-like fashion) as buttressing ice is lost. In (E), the effect of multiple generations of contraction-crack polygons and sand wedges produces an increasingly chaotic arrangement of the sand wedge facies; relict and active sand wedges truncate all facies of Mullins till. In (F), the cartoon shows a typical plain view image of active (dark brown) and relict (light brown) sand wedges; relict sand wedges (e.g., relict polygons) are typically only viewed in stratigraphic section. Panels (G)–(I) show textural characteristics for each of the three facies of Mullins till, as observed in thin-section analyses. In (G), the fresh facies shows angular grains with diagnostic green and maroon siltstone fragments, most of which are likely derived from the Arena Sandstone Formation at the valley headwall. Using MatLab image analyses, the average porosity of the fresh facies is estimated at ~29.5%. (For all estimates of porosity, a minimum of six image analyses were performed for each facies.) (H) The weathered facies of Mullins till; note the increase in stained grains (with iron oxides) over that seen in the fresh facies; the average porosity of the weathered facies is estimated at ~29%. (I) The sand-wedge facies; average porosity is estimated at ~31%.

4.4. Spatial variation in the distribution of each facies

4.4.1. Weathered facies

The weathered facies is present in all exposures of Mullins till. By definition, it is the only facies present where the till is ≤ 20 cm thick (as occurs in most of Mullins Valley; Fig. 6).

4.4.2. Fresh facies

The fresh facies is uncommon. It is first observed at the base of soil pits ~3 km from the valley headwall, where Mullins till thickens consistently beyond ~20 cm. The fresh facies is spatially restricted (not laterally extensive) and commonly truncated by active and/or

relict sand wedges. In all cases, the fresh facies rests directly on glacier ice; its maximum observed thickness is ~40–50 cm.

4.4.3. Sand-wedge facies

The percentage of sand-wedge facies comprising Mullins till increases with distance downglacier. The increase reflects the growing number of relict wedges that arise with the addition of each new generation of contraction-crack polygons. For sections of Mullins till most affected by multiple generations of contraction-crack polygons (e.g., on the floor of central Beacon Valley), the observed sedimentary architecture may consist of ~65% sand-wedge facies (the

Table 2
Physical attributes of till facies, Mullins Valley.

Facies	Porosity ^a (std deviation)	Grain size analysis (mean, %)			Lithology (>16 mm) dolerite:sandstone:siltstone ^b	Impact chips	Munsell color
		Gravel	Sand	Mud			
Weathered	29.0% (2.9%)	25.2	72.9	1.9	96:04:00	Absent	10YR 5/4–5YR 5/7
Fresh	29.5% (2.1%)	45.3	49.7	5.0	93:06:01	Present	2.5Y 7/2
Sand-Wedge	31.0% (2.4%)	3.1	92.9	4.0	99:01:00	Absent	10YR 5/4

^a Reported values reflect the smallest measured variation among facies.

^b Green and maroon siltstone, most probably derived from rockfall from the Arena Sandstone.

vast majority of which are relict wedges), 15% weathered facies, and 20% fresh facies (see also Fig. 6 for additional details).

4.5. Microclimate variation

Tables 1a, 1b, 1c summarizes our observations and meteorological data collected between December 2004 and December 2009 (Fig. 7). An important point is that summertime environmental conditions vary appreciably along the length of Mullins Glacier. For example, the maximum summertime air temperature (December, January, and February) recorded at 10 cm above the till in upper Mullins Valley (site 2, 1524 m elevation) reached 1.6 °C, while at the glacier terminus (site 5, 1272 m elevation) the maximum temperature reached 5 °C. All recorded atmospheric temperature maxima were short lived, lasting

only a few hours; and none of our five monitored sites showed positive-degree days for any portion of the study interval (2004–2009). At all measured locations, the buried surface of Mullins glacier was dry and <<0 °C.

Measured values for relative humidity (RH) revealed a general trend toward higher values with increasing elevation, with a mean of ~48% at Mullins terminus (site 5, 1272 m elevation) and 60% at 1550 m elevation in upper Mullins Valley (site 1). The higher values in upper Mullins Valley likely reflect the persistence of low clouds in that region (as observed in the field).

Apart from abrupt spikes in soil moisture that arise from minor snowmelt at the margin of solar-heated rocks, all facies within Mullins till contain <5% gravimetric water content (GWC). The infrequent snowmelt along solar-heated rocks generates a moist (but not

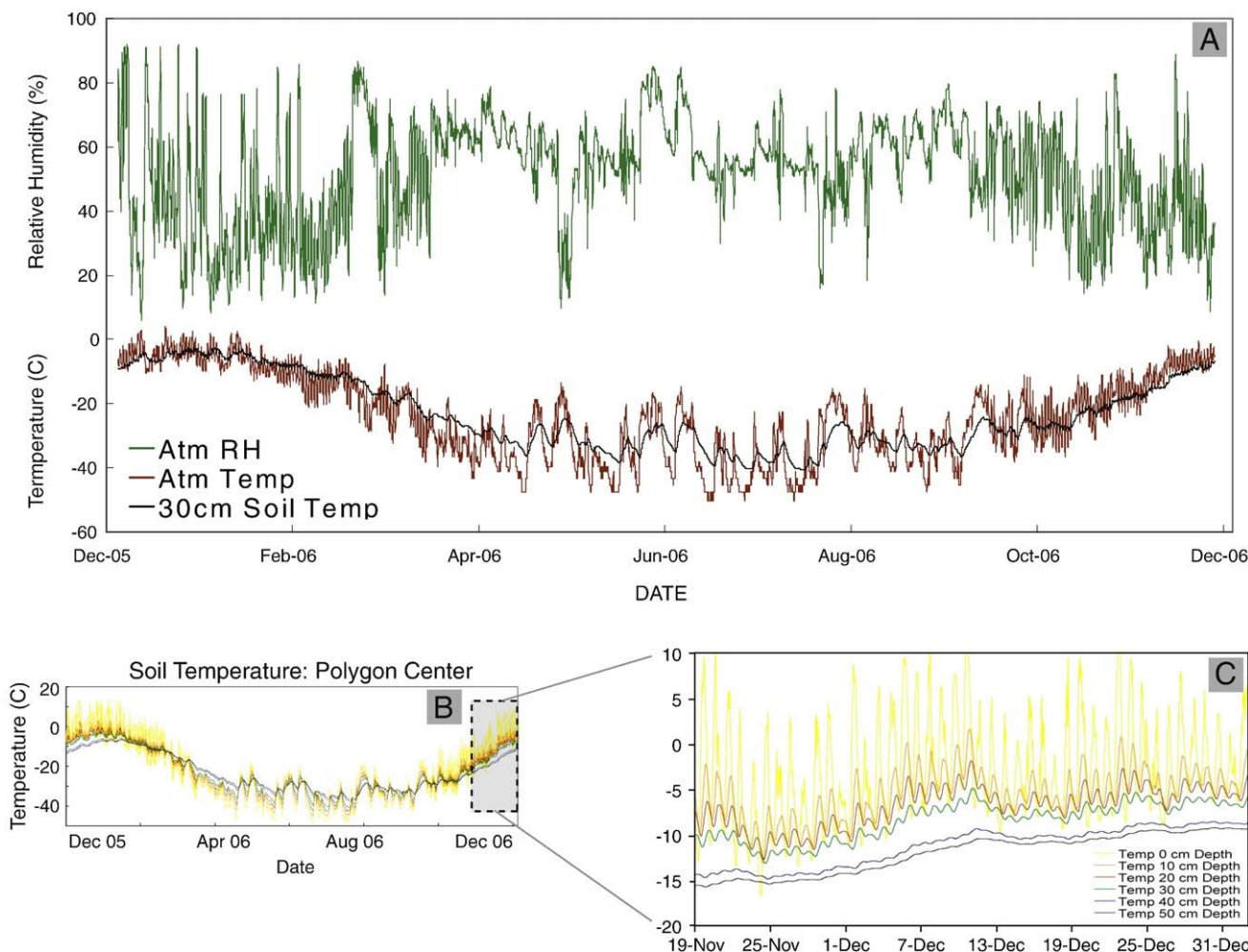


Fig. 7. A 12-month data set of (A) atmospheric data and (B) soil temperature recorded at Mullins terminus meteorological station (site 5; see Fig. 2C). (C) Blow-up of soil temperature profile data. Note progressive dampening of the thermal wave with depth; daily variations are essentially absent at depths of ≥ 50 cm. Ground surface temperatures exceed 0 °C by several degrees because of solar warming of low-albedo rocks, but temperatures at depths > 10 cm consistently remain below 0 °C.

saturated) wetting front (<10% GWC) that reaches a maximum depth of ~15 cm; visual inspection revealed that most of this moisture is quickly lost via evaporation within hours after infiltration. In most cases, snowfall at the ground surface sublimates before melting (e.g., Fountain et al., 2010).

5. Numerical modeling

5.1. Assumptions and model format

Vapor fluxes through cold and dry tills are governed primarily by two mechanisms: molecular diffusion of vapor in pore spaces and advection of air through the material. Other forces influence vapor transport, including osmotic pressure and nonisothermal vapor flux; but it has been reported that Fickian diffusion processes dominate transport in extreme cold environments (Chevrier et al., 2007, 2008; Hudson et al., 2007). Our vapor-diffusion model ignores the very minor effects of Knudsen diffusion and does not specifically track vapor density beyond saturation (as may occur with the formation of hoar frost). Results, however, can be used to infer times when secondary ice would likely form in pore spaces within the Mullins till. Such secondary ice would decrease till porosity, retard vapor diffusion, and cause our model to overestimate ice loss; hence our modeled values for ice loss presented below are most appropriately viewed as maxima, not minima. Lastly, we do not consider the effects of adsorption/desorption of water vapor on soil particles in this treatment. Although such processes likely play a role in modulating vapor diffusion, recent studies suggest that the effects are typically short lived and most probably of second-order importance; further research is required (Schorghofer and Aharonson, 2005).

The molecular diffusion of water vapor in pores in Mullins till is expressed using Fick's Second Law,

$$\frac{\partial \rho}{\partial t} = D \frac{\partial^2 \rho}{\partial z^2} \quad (1)$$

where ρ represents water vapor density, t the time, D the diffusivity of water vapor ($0.16 \text{ cm}^2 \text{ s}^{-1}$) (Mellon and Jakosky, 1993; McKay et al., 1998), and z is equal to distance. To address vapor diffusion through a porous medium, we then introduce variables to express porosity, ϕ , and tortuosity, b (Eq. 2), into Eq. (1). Vapor diffusion flux can now be expressed as

$$\frac{\partial \rho}{\partial t} = \left(\frac{\phi D}{b}\right) \cdot \frac{\partial^2 \rho}{\partial z^2} \quad (2)$$

The vapor density for boundary and initial conditions is calculated from the water vapor pressure (e), which can be derived using the Clausius–Clapeyron equation

$$e = e_0 \cdot \exp\left[\frac{L}{R_v} \cdot \left(\frac{1}{T_0} - \frac{1}{T}\right)\right] \cdot \frac{RH}{100} \quad (3)$$

where e_0 and T_0 are constant parameters equal to 0.611 kPa and 273 K, respectively; L/R_v is equal to the latent heat of deposition divided by the gas constant of water vapor which equals 6139 K; and T and RH are the HOBO™ Smart Sensor measured temperature and the relative humidity, respectively. The relationship between vapor pressure and vapor density can be calculated using the ideal gas law as follows:

$$e = \rho R_v T \quad (4)$$

where the equation is solved for the vapor density. We solve Eq. (2) with the implicit finite differences method to calculate vapor fluxes

through the till using 1 cm grid spacing. Ice loss is calculated from the net vapor flux at the ice–till interface.

We assume that the temperature of air in pores within Mullins till is the same as that recorded for surrounding sediment. In the rare cases where soil temperatures were unavailable at depth, we calculated the expected soil temperatures at depth by propagating measured soil surface temperatures using the following one-dimensional heat diffusion equation solved using finite differences:

$$\frac{\partial T}{\partial t} = \kappa \frac{\partial^2 T}{\partial z^2} \quad (5)$$

where T represents temperature, t is time, κ is the thermal diffusivity, and z is depth. Thermal diffusivity for the various facies of Mullins till was calculated from our measured data as

$$\kappa = \frac{\pi}{P} \left(\frac{z_2 - z_1}{\ln(\delta_1 / \delta_2)}\right)^2 \quad (6)$$

where P is the period, and δ is half-amplitude of the temperature variation at depth z . Calculated thermal diffusivities are $2.3 \times 10^{-7} \text{ m}^2 \text{ s}^{-1}$ for the weathered facies; $8.8 \times 10^{-7} \text{ m}^2 \text{ s}^{-1}$ for the fresh facies; and $5.3 \times 10^{-7} \text{ m}^2 \text{ s}^{-1}$ for both the sand-wedge facies (same values for active and relict sand wedges). These values fall within the range of thermal diffusivities calculated for various sediments throughout the Dry Valleys region (Campbell et al., 1997; Campbell and Claridge, 2006). Boundary temperature conditions for the ice surface were established from ice core temperatures at 5 m depth.

The boundary conditions for relative humidity (RH) are set to the measured value for atmospheric temperature at the till surface and are assumed to be 100% just above the buried ice surface. Initial conditions include a linear function of RH between these two boundary conditions. The model then solves Eq. (2) to determine vapor density as a function of depth and computes cumulative vapor flux.

5.2. Modeling exercise 1: elucidating the role of till facies on ice sublimation

5.2.1. Strategy

To examine the extent to which changes in the porosity and thermal diffusivity of facies within Mullins till alter sublimation of underlying ice, we modeled ice losses beneath three simulated till sections: one in which the till was composed entirely of the fresh facies; a second in which it was composed entirely of the weathered facies; and a third in which it was composed entirely of the sand-wedge facies. For all model runs, till thickness was arbitrarily set at 50 cm, and meteorological forcing came from data collected at the Mullins terminus (site 5) in 2006 (Tables 1a, 1b, and 1c). Subsurface temperature profiles were created for each model run according to thermal diffusivities calculated in Eq. (6) above.

5.2.2. Results

The results show that variations in till texture and thermal diffusivity impact vapor diffusion and loss of buried ice. Annual losses beneath the fresh, weathered, and sand-wedge facies are 0.0603, 0.0601, and 0.0636 mm a^{-1} , respectively. Setting sublimation losses beneath the fresh facies as a base level value and assigning percentages (higher or lower than base level) for the remaining two facies indicates that ice loss is greater beneath the sand-wedge facies by 5.47% and lower beneath the weathered facies by 0.33%. Although these net deviations are relatively small, they help explain some of the meter-scale topographic relief observed at the surface of buried glacier ice in this region (e.g., Linkletter et al., 1973; Bockheim, 2002; Marchant et al., 2002; Sletten et al., 2003). For example, over timescales of 10^5 years, the increased sublimation beneath active sand wedges could result in the development of marginal polygon

troughs that are depressed ~1.0 m relative to elevated polygon centers (Fig. 6). The implication is that enhanced vapor diffusion through “porous” sand wedges may contribute to the development of high-centered polygons as noted in Marchant et al. (2002).

5.3. Modeling exercise 2: determining the role of facies thickness on ice sublimation

5.3.1. Strategy

In this series of tests, we determine the critical thickness, T_c , that effectively reduces annual ice loss via sublimation to near-zero levels (asymptotically approaching zero). To determine T_c , we modeled net ice loss beneath increasingly thick Mullins till. The uppermost 15 cm of Mullins till was composed of the weathered facies, with the fresh facies (only) occurring at greater depths. Meteorological input come from data collected halfway down Mullins Valley (site 4).

5.3.2. Results

Results show that as the till thickens from 10 to 50 cm there is a rapid decline in annual net ice loss. Ice loss approaches zero with a T_c of 145 cm (Fig. 8).

5.4. Modeling exercise 3: resolving spatial variations in ice sublimation along Mullins Glacier

5.4.1. Strategy

To determine the magnitude of spatial variation in ice sublimation along the debris-covered portions of Mullins Glacier, we calculated sublimation losses during a three-week summertime period at five localities along Mullins Glacier (3–24 December 2004; Tables 1a, 1b, and 1c); where longer term meteorological data were available, we also calculated net ice losses over a calendar year (2006) (Tables 1b and 1c). The sites examined cover an elevation range of ~350 m, and multiple facies of Mullins till are present at most locales. All sites are located along the glacier centerline. Modeled ice losses are reported in Table 3, with site-specific details provided below.

5.4.2. Results

Site 1 is located ~2500 m from the headwall of Mullins Valley (1550 m elevation). Mullins till is 10 cm thick and composed entirely of the

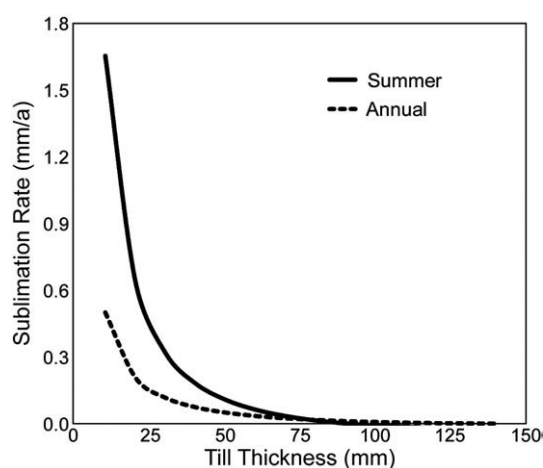


Fig. 8. Model results showing the variation in rates of buried ice sublimation as a function of increasing till thickness. Rates of annual sublimation asymptote to zero with increasing till thickness; the plot also emphasizes that, for sections of Mullins till <25 cm thick, sublimation rates are considerably higher during summer months (December, January, February: DJF) than at other times of the year. As the till thickens, however, the relative importance of sublimation in DJF tends to diminish; the most likely explanation is that sublimation losses continue into the austral fall (e.g., March, April, and May) as a consequence of the longer duration penetration of the summertime thermal wave passing through thick exposures of Mullins till.

weathered facies. The mean calculated vapor flux is $2.5 \times 10^{-8} \text{ kg m}^{-2} \text{ s}^{-1}$ in the outward (upward to the atmosphere) direction. This yields a net ice loss of $4.5 \times 10^{-2} \text{ mm}$ during the 21-day summer interval (Table 3). In our calculations, a positive flux denotes outward flow toward the atmosphere, whereas a negative flux represents downward vapor movement toward the buried ice surface.

Site 2 site is located ~3000 m from the valley headwall (1524 m elevation). Mullins till is 18 cm thick and composed of the weathered facies to a 10-cm depth and the relict sand wedges facies thereafter. The calculated mean vapor flux is $9.9 \times 10^{-9} \text{ kg m}^{-2} \text{ s}^{-1}$, yielding a net ice loss of $1.8 \times 10^{-2} \text{ mm}$ during the three-week summer interval (Table 3). Vapor consistently flowed outward toward the atmosphere. Long-term ice loss, as calculated during the 2006 calendar year, was 0.1220 mm (Table 3).

Site 3 is situated ~3800 m from the valley headwall (1442 m elevation). Mullins till is 22 cm thick and consists of the weathered facies to ~15 cm and the relict sand-wedge facies thereafter. The calculated mean vapor flux is $1.8 \times 10^{-8} \text{ kg m}^{-2} \text{ s}^{-1}$ (Table 3). This yields a net ice loss of $3.2 \times 10^{-2} \text{ mm}$ during the three-week summer interval; vapor consistently flowed outward toward the atmosphere.

Site 4 is located 4500 m from the valley headwall (1374 m elevation). The 25-cm thick section is composed of the weathered facies to a 14-cm depth and the fresh facies thereafter. The mean vapor flux is $1.2 \times 10^{-8} \text{ kg m}^{-2} \text{ s}^{-1}$, yielding a net ice loss of $2.1 \times 10^{-2} \text{ mm}$ for the three-week summer interval (0.1579 mm for the measured 2006 calendar year) (Table 3). Vapor exhibited bidirectional flow (moving inward and outward) during the 21-day study interval.

Site 5 is located 7800 m from the valley headwall in central Beacon Valley (1272 m elevation). The 50-cm thick till section consists of the weathered facies to a depth of 15 cm and the fresh facies thereafter. The mean vapor flux is $3.7 \times 10^{-9} \text{ kg m}^{-2} \text{ s}^{-1}$, yielding a net ice loss of $6.7 \times 10^{-3} \text{ mm}$ during the three-week summer interval (0.0656 mm for the measured 2006 calendar year) (Table 3). The vapor flowed both into and out of the till during the 21-day study interval.

Three conclusions arise from these model results. First, sublimation rates decrease with increasing distance downglacier. The decrease in net sublimation is due to progressive thickening of Mullins till, which more than offsets predicted gains in ice sublimation that are expected to occur from the greater concentration of porous sand-wedge deposits in the down-ice direction (see also Section 4.4; Fig. 9). Second, for exposures of Mullins till >25 cm in thickness, complex thermal variations result in both outward and inward vapor fluxes; a similar conclusion for bidirectional vapor flow was reached by Kowalewski et al. (2006), who showed that downward vapor fluxes through granite drift in central Beacon Valley could produce thin layers of accretion ice at the buried surface of relict ice from Taylor Glacier. Third, although sublimation losses are greatest during summer months, the relative importance of December, January, and February (DJF) losses on net-annual ablation varies with till thickness. Apparently, DJF ice losses are greatest in regions with thin till (<25 cm thick), where the impact of summertime warming at the buried ice surface is felt most quickly. At till thicknesses >40 cm, delayed warming at the buried ice surface extends the season of maximum ice loss beyond DJF.

6. Discussion

6.1. Implications for long-term preservation of glacier ice

The potential for ancient buried glacier ice in the Dry Valleys has been debated for years (e.g., see Sugden et al., 1995; Hindmarsh et al., 1998; McKay et al., 1998; Schaefer et al., 2000; Stone et al., 2000; Marchant et al., 2002; Sletten et al., 2003; Ng et al., 2005; Hagedorn et al., 2007, 2010; McKay, 2009; Schorghofer, 2009; Morgan et al., 2010). Recent findings from the planetary-science community, which suggest that far older ice survives beneath thin debris on Mars, have

Table 3
Spatial variation in ice sublimation, Mullins Glacier.

Meteorological station	Till thickness (m)	Mean vapor transport rates (mm/s)	Minimum vapor transport rates (mm/s) ^a	Maximum vapor transport rates (mm/s) ^a	Summertime vapor flow direction	Summertime study interval ice loss (mm) ^b	Net annual ice loss (mm)	% Annual sublimation during 3-week study interval
Site 1	0.10	2.5×10^{-8}	1.1×10^{-8}	4.3×10^{-8}	↑	0.0452	n/a	n/a
Site 2	0.18	9.9×10^{-9}	2.5×10^{-9}	2.6×10^{-8}	↑	0.0180	0.1220	14.8%
Site 3	0.22	1.8×10^{-9}	5.6×10^{-9}	2.9×10^{-8}	↑	0.0322	n/a	n/a
Site 4	0.25	1.2×10^{-8}	-9.6×10^{-9}	1.5×10^{-8}	↑↓	0.0209	0.1579	13.2%
Site 5	0.50	3.7×10^{-9}	-9.5×10^{-9}	1.0×10^{-8}	↑↓	0.0067	0.0656	10.2%

^a Max vapor is always in outward direction; negative values represent vapor flux toward the ice.

^b Summertime study interval from 3 to 24 December 2006.

served to intensify the debate (Mellon and Jakosky, 1995; Boynton et al., 2002; Feldman et al., 2002; Mitrofanov et al., 2002; Head and Marchant, 2003; Schorghofer and Aharonson, 2005; Head et al., 2006; Chevrier et al., 2008; Holt et al., 2008; Mellon et al., 2008; Plaut et al., 2009; see also Dickinson and Rosen, 2003). Our modeling results show that annual ice loss at the Mullins terminus (site 5) is $\sim 6.6 \times 10^{-5} \text{ m a}^{-1}$. Without influx of ice from upvalley and assuming long-term climate conditions similar to today, the results suggest complete loss of Mullins Glacier ice in central Beacon Valley within $\sim 2.5 \text{ Ma}$ (150-m thick glacier ice less $\sim 6.6 \times 10^{-5} \text{ m a}^{-1}$). We recognize the strong likelihood of the influx of ice from upvalley (at a minimum to compensate for ice surface lowering in central Beacon Valley); but without specific details on the magnitude of potential influx, we simply consider the ice as a stagnant block, without lateral influx or outflow, and one in which ice is lost or gained only by vapor diffusion through overlying Mullins till. Given this framework, we seek to understand the specific environmental conditions that could result in zero ice loss—an apparently extreme condition, but one fully consistent with preservation of eight-million-year-old ice (Sugden et al., 1995).

For this exercise, we modified soil/ice surface temperatures and atmospheric RH at the Mullins terminus site (site 5) so that sublimation losses over our 21-day summer interval (Tables 1a, 1b, 1c) would equal zero; changes in subsurface temperatures and RH were treated as independent parameters (Fig. 10). Although relatively short in duration, the 21-day summertime interval captures the maximum period of annual ice sublimation (e.g., Kowalewski et al., 2006, and below), and so our results highlight the most extreme meteorological changes that are required to halt buried ice sublimation at site 5.

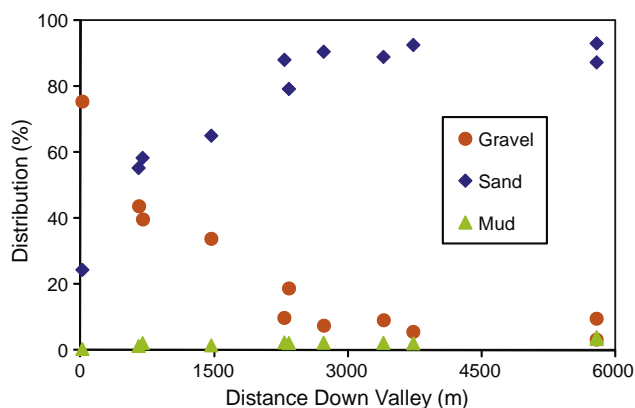


Fig. 9. The relative proportion of gravel, sand, and mud in Mullins till (averaged over all facies) as a function of increasing distance downvalley. The increased percentage of sand-sized grains in the down-ice direction is a result of the greater concentration of relict sand-wedge deposits that arise with the addition of each new generation of contraction-crack polygons.

6.1.1. The change in summertime soil and ice surface temperature required to achieve zero ice loss

To determine the changes in soil and ice surface temperatures required to achieve zero ice loss at site 5 (as departures from our measured values over the 21-day study interval, Table 3), we adjusted the measured soil and ice surface temperature at site 5 in increments of 1 °C (at all depths) and recalculated vapor densities (Eqs. (3) and (4)) and sublimation losses (maintaining atmospheric RH at measured values). Results suggest that sublimation is zero with a decrease of 6.4 °C at all measured depths.

6.1.2. The change in summertime RH required to achieve zero ice loss

To determine the change in RH required to achieve zero ice loss for our three-week summer interval at site 5, we ran a series of model experiments that retained existing soil and ice temperatures but incrementally increased atmospheric RH. Vapor densities were not allowed to exceed saturation. Results show that a net increase in RH of 31% (from 44% to 75%) would result in zero ice loss over the 21-day study interval. Fig. 10 shows the deviations required for both soil temperature and vapor density that would result in negligible ice loss (or even ice gain) over the 21-day study interval.

The modeling results highlight the sensitivity of ice loss to environmental change. The results suggest that an increase in cloud cover might be sufficient to halt summertime ice loss beneath Mullins till in central Beacon Valley. An increase in cloud cover would likely result in cooler ground surface temperatures and, if associated with increased precipitation as one might expect, higher values for atmospheric RH. In addition, the documented potential for infiltration

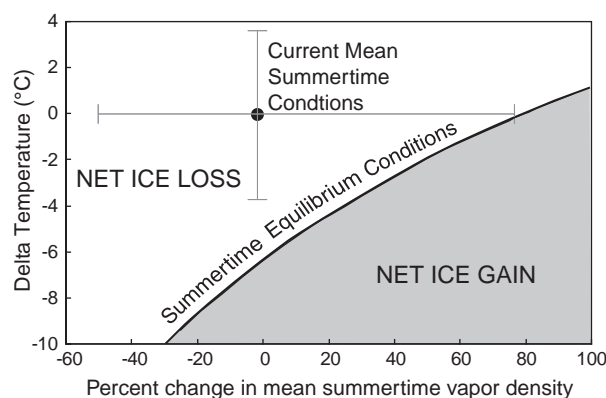


Fig. 10. Modeled hypothetical stability field for buried glacier ice beneath 50 cm of Mullins till (till-texture parameters and meteorological conditions are from the Mullins Terminus, site 5; see Fig. 2). The plot shows that under current summertime conditions (i.e., the black dot marking the spot at which delta temperature and delta vapor density both equal 0), the buried ice surface is unstable and undergoes sublimation (the bars show the range in mean daily DJF temperatures and vapor density for this site). The results suggest that as soil and ice surface temperatures drop by $\sim 6.5 \text{ °C}$, summertime ice loss reaches zero. Likewise, net summertime sublimation drops to zero (yielding stable ice conditions) if RH increases by $\sim 30\%$. The thin black line between the shaded region of net ice gain and net ice loss shows the range of values for Delta T and Delta VD% (vapor density) that are consistent with a stable ice surface.

of shallow snowmelt would be an additional factor retarding net ice loss (e.g., Kowalewski et al., 2006; Hagedorn et al., 2007, 2010; McKay, 2009; Schorghofer, 2009). Finally, using a two dimensional model for vapor diffusion that included the effects of rocky surface pavements and salt-cemented horizons, Kowalewski and Marchant (in review) showed that sublimation losses for buried ice associated with Taylor Glacier in central Beacon Valley (e.g., beneath granite drift; Fig. 2C) dropped to zero with either a slight reduction in mean annual atmospheric temperature of 1.9 °C or a very modest 12% increase in mean annual RH.

6.2. Is the sublimation response to past and/or future climate change uniform across Mullins Glacier?

The above set of experiments focused solely on ice loss at a single locality, the terminus of Mullins Glacier (site 5). Here, we consider whether the model results for the terminus can be applied uniformly across the surface of Mullins Glacier, or whether different parts of the glacier surface show varying responses to atmospheric forcing. To answer this question, we performed a series of climate sensitivity tests for various localities along Mullins Glacier. Among the results presented in Fig. 11 is that a uniform increase in soil temperatures of 2 °C (at all depths, including the ice surface) results in negligible change in ice sublimation at Mullins terminus (site 5), but a 27% increase in ice loss in upper Mullins Valley (site 1). Fig. 11 also shows the results of similar tests for changes in RH. The results highlight the spatially non-uniform response of ice sublimation to a single change in atmospheric forcing and emphasize the first-order control of till thickness on subjacent ice loss.

7. Summary and conclusions

- (i) Mullins Glacier, ~8 km in length, originates as a small alpine glacier fed by local snowfall at the head of Mullins Valley. A combination of rockfall onto the ice accumulation zone, along with progressive sublimation and concentration of englacial debris at the ice surface, has produced Mullins till (a supraglacial till) that retards sublimation of underlying ice.
- (ii) We distinguish three textural facies within Mullins till: a weathered facies that represents oxidation of iron-bearing minerals and physical disintegration of surface rocks; a sand-wedge facies that represents episodic infill of thermal contraction cracks at polygon margins; and a relatively rare, fresh facies that represents the direct contribution of englacial debris (fresh-appearing rockfall debris) added to the base of Mullins till as ice sublimates.
- (iii) Our modeling studies indicate sublimation losses beneath the three facies of Mullins till differ by 5.5%; losses are greatest beneath the sand-wedge facies and lowest beneath the weathered facies. Over timescales of 10^5 years, accelerated rates of sublimation beneath the relatively porous sand-wedge facies contributes to the development of deep (meter scale) surface troughs. The implication is that enhanced vapor diffusion through sand wedges may contribute to the development of high-centered polygons as noted in Marchant et al. (2002).
- (iv) Under current environmental forcing, stagnant regions of Mullins Glacier sublime (lower) by $\sim 6.6 \times 10^{-5} \text{ m a}^{-1}$. Without influx of ice from upvalley, Mullins ice in central Beacon Valley would sublime completely within $\sim 2.5 \text{ Ma}$ (150-m thick glacier ice less $\sim 6.6 \times 10^{-5} \text{ m a}^{-1}$).
- (v) Our results suggest that summertime ice loss could drop to zero given either a summertime decrease in till and ice surface temperatures of 6.4 °C or a 31% increase in atmospheric RH. We suggest that such conditions could be achieved with an increase in summertime cloud cover over Beacon Valley.
- (vi) Subtle changes in microclimate parameters yield very different sublimation responses along the length of Mullins Glacier. For example, a uniform increase in soil and ice surface temperatures of 2 °C results in negligible change in ice sublimation at Mullins terminus, but a 27% increase in the rate of buried ice sublimation in upper Mullins Valley. Such spatial variation in response to environmental forcing could help explain the occurrence of beheaded, debris-covered glaciers, e.g., those glaciers that emanate from deep hollows formerly occupied with ice minimally covered with sublimation till (e.g., Marchant and Head, 2007; Head et al., 2008).

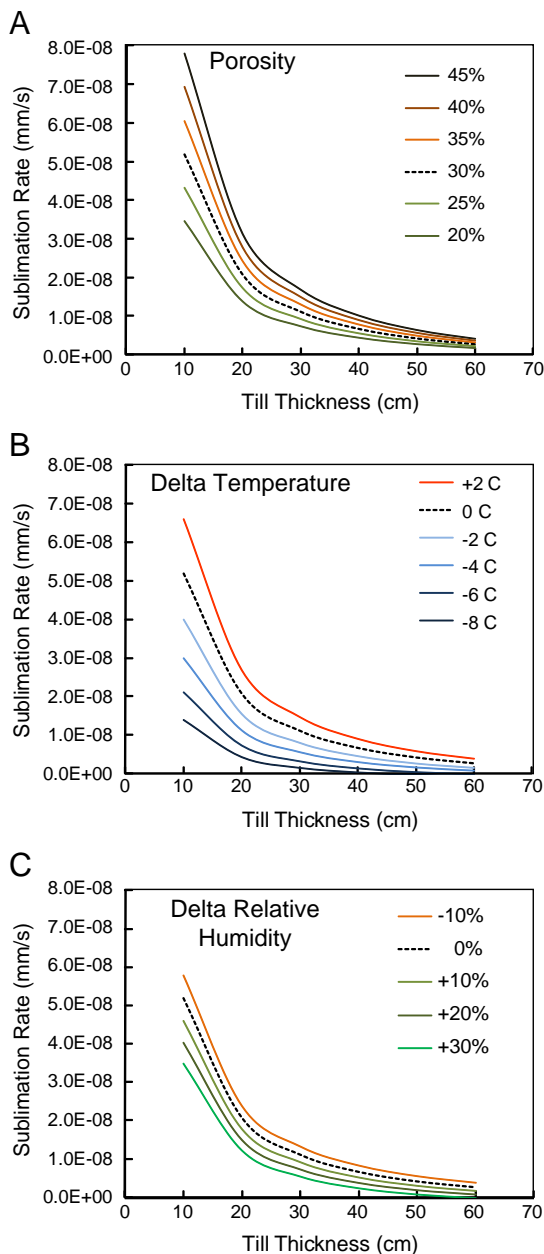


Fig. 11. Calculated rates for ice sublimation as a function of varying porosity, till temperature, and atmospheric RH for a variety of till thickness values. (A) Results from sensitivity tests that highlight the relationship between sublimation rate and till porosity for varying thicknesses of Mullins till. Ice beneath thin till is more responsive to changes in till porosity than that beneath thick till. (B) Results from sensitivity tests showing the relationship between sublimation rate and soil/ice surface temperatures for various till thicknesses. Colder ground temperatures suppress sublimation; shallow ice is more sensitive to climatic change than is ice buried beneath thick till. (C) Results showing the relationship between sublimation rate and RH for various till thicknesses. Higher RH yields lower sublimation rates; shallow ice shows greater response to changes in RH. In all tests, the dashed line represents modern, baseline conditions; see text for explanation.

Acknowledgements

Funding for this research was provided by NSF Polar Programs Grants ANT-0636705 and ANT-0944702 to DRM and NSF Post Doctoral Fellowship 0851695 to DEK. We thank Adam Lewis, David Shean, Joe Levy, Gareth Morgan, Sean Mackay, James Dickson, and Jen Lamp for excellent discussions and assistance in the field.

References

- Ackert, R.P., 1998. A rock glacier/debris-covered glacier system at Galena Creek, Absaroka Mountains, Wyoming. *Geografiska Annaler* 80 (A), 267–276.
- Augustin, L., Barbante, C., Barnes, P.R.F., Barnola, J.M., Bigler, M., Castellano, E., Cattani, O., Chappellaz, J., Dahljensen, D., Delmonte, B., Dreyfus, G., Durand, G., Falourd, S., Fischer, H., Flückiger, J., Hansson, M.E., Huybrechts, P., Jugie, R., Johnsen, S.J., Jouzel, J., Kaufmann, P., Kipfstuhl, J., Lambert, F., Lipenkov, V.Y., Littot, G.V.C., Longinelli, A., Lorrain, R., Maggi, V., Masson-Delmotte, V., Miller, H., Mulvaney, R., Oerlemans, J., Oerter, H., Orlandini, G., Parrenin, F., Peel, D.A., Petit, J.R., Raynaud, D., Ritz, C., Ruth, U., Schwander, J., Siegenthaler, U., Souchez, R., Stauffer, B., Steffensen, J.P., Stenni, B., Stocker, T.F., Tabacco, I.E., Udisti, R., van de Wal, R.S.W., van den Broeke, M., Weiss, J., Wilhelms, F., Winther, J.G., Wolff, E.W., Zucchelli, M., 2004. Eight glacial cycles from an Antarctic ice core. *Nature* 429 (6992), 623–628.
- Berg, T.E., Black, R.F., 1966. Preliminary measurements of growth of nonsorted polygons, Victoria Land, Antarctica. In: Tedrow, J.C.F. (Ed.), *Antarctic Soils and Soil Forming Processes: American Geophysical Union Antarctic Research Series* 8, Washington, D.C., pp. 61–108.
- Bidle, K.D., Lee, S., Marchant, D.R., Falkowski, P.G., 2007. Fossil genes and microbes in the oldest ice on Earth. *Proceedings of the National Academy of Sciences of the United States of America* 104 (33), 13455–13460.
- Bockheim, J.G., 2002. Landform and soil development in the McMurdo Dry Valleys, Antarctica: a regional synthesis. *Arctic and Antarctic Research* 34 (3), 308–317.
- Bockheim, J.G., 2010. Evolution of desert pavements and the vesicular layer in soils of the Transantarctic Mountains. *Geomorphology* 118, 433–443.
- Bockheim, J.G., Campbell, I.B., McLeod, M., 2007. Permafrost distribution and active-layer depths in the McMurdo Dry Valleys, Antarctica. *Permafrost and Periglacial Processes* 18, 217–227. doi:10.1002/ppp.588.
- Bockheim, J.G., Kurz, M.D., Soule, S.A., Burke, A., 2009. Genesis of active sand-filled polygons in lower and central Beacon Valley, Antarctica. *Permafrost and Periglacial Processes* 20, 295–308. doi:10.1002/ppp.661.
- Boynton, W.V., Feldman, W.C., Squyres, S.W., Prettyman, T.H., Bruckner, J., Evans, L.G., Reedy, R.C., Starr, R., Arnold, J.R., Drake, D.M., Englert, P.A.J., Metzger, A.E., Mitrofanov, I., Trombka, J.I., d'Uston, C., Wanke, H., Gasnault, O., Hamara, D.K., Janes, D.M., Marcialis, R.L., Maurice, S., Mikheeva, I., Taylor, G.J., Tokar, R., Shinohara, C., 2002. Distribution of hydrogen in the near surface of Mars: evidence for subsurface ice deposits. *Science* 297 (5578), 81–85.
- Campbell, D.I., MacCulloch, R.J.L., Campbell, I.B., 1997. Thermal regimes of some soils in the McMurdo Sound region, Antarctica. In: Lyons, W.B., Howard-Williams, C., Hawes, I. (Eds.), *Ecosystem Processes in Antarctica Ice-free Landscapes*. Balkema, Rotterdam, The Netherlands, pp. 45–55.
- Campbell, I.B., Claridge, G.G.C., 2006. Permafrost properties, patterns and processes in the Transantarctic Mountains region. *Permafrost and Periglacial Processes* 17 (3), 215–232.
- Chevrier, V., Sears, D.W.G., Chittenden, J.D., Roe, L.A., Ulrich, R., Bryson, K., Billingsley, L., Hanley, J., 2007. Sublimation rate of ice under simulated Mars conditions and the effect of layers of mock regolith JSC Mars-1. *Geophysical Research Letters* 34 (2). doi:10.1029/2006GL028401.
- Chevrier, V., Ostrowski, D.R., Sears, D.W.G., 2008. Experimental study of the sublimation of ice through an unconsolidated clay layer: implications for the stability of ice on Mars and the possible diurnal variations in atmospheric water. *Icarus* 196 (2), 459–476.
- Dickinson, W.W., Rosen, M.R., 2003. Antarctic permafrost: an analogue for water and diagenetic minerals on Mars. *Geology* 31 (3), 199–202.
- Doran, P.T., McKay, C.P., Clow, G.D., Dana, G.L., Fountain, A.G., Nylen, T., Lyons, W.B., 2002. Valley floor climate observations from the McMurdo Dry Valleys, Antarctica 1986–2000. *Journal of Geophysical Research*, [Atmospheres] 107, D244772. doi:10.1029/2001JD002045.
- Feldman, W.C., Boynton, W.V., Tokar, R.L., Prettyman, T.H., Gasnault, O., Squyres, S.W., Elphic, R.C., Lawrence, D.J., Lawson, S.L., Maurice, S., McKinney, G.W., Moore, K.R., Reedy, R.C., 2002. Global distribution of neutrons from Mars: results from Mars Odyssey. *Science* 297 (5578), 75–78.
- Fountain, A.G., Nylen, T.H., Monaghan, A., Basagic, H.J., Bromwich, D., 2010. Snow in the McMurdo Dry Valleys, Antarctica. *International Journal of Climatology*. doi:10.1002/joc.1933.
- Hagedorn, B., Sletten, R.S., Hallet, B., 2007. Sublimation and ice condensation in hyperarid soils: modeling results using field data from Victoria Valley, Antarctica. *Journal of Geophysical Research, Earth Surface* 112 (F3). doi:10.1029/2006JF000580 F03017.
- Hagedorn, B., Sletten, R.S., Hallet, B., McTigue, D.F., Steig, E.J., 2010. Ground ice recharge via brine transport in frozen soils of Victoria Valley, Antarctica: insights from modeling 18 O and D profiles. *Geochimica et Cosmochimica Acta* 74, 435–448.
- Head, J.W., Marchant, D.R., 2003. Cold-based mountain glaciers on Mars: western Arsia Mons. *Geology* 31 (7), 641–644.
- Head, J.W., Marchant, D.R., Agnew, M.C., Fassett, C.I., Kreslavsky, M.A., 2006. Extensive valley glacier deposits in the northern mid-latitudes of Mars: evidence for Late Amazonian obliquity-driven climate change. *Earth and Planetary Science Letters* 241 (3–4), 663–671.
- Head, J.W., Marchant, D.R., Kreslavsky, M.A., 2008. Formation of gullies on Mars: link to recent climate history and insolation microenvironments implicate surface water flow origin. *Proceedings of the National Academy of Sciences of the United States of America* 105 (36), 13258–13263. doi:10.1073/pnas.0803760105.
- Hindmarsh, R.C.A., Van der Wateren, F.M., Verbers, A., 1998. Sublimation of ice through sediment in Beacon Valley, Antarctica. *Geografiska Annaler Series A-Physical Geography* 80A (3–4), 209–219.
- Holt, J.W., Safaenili, A., Plaut, J.J., Head, J.W., Phillips, R.J., Seu, R., Kempf, S.D., Choudhary, P., Young, D.A., Putzig, N.E., Biccari, D., Gim, Y., 2008. Radar sounding evidence for buried glaciers in the southern mid-latitudes of Mars. *Science* 322, 1235–1238. doi:10.1126/science.1164246.
- Hudson, T.L., Aharonson, O., Schorghofer, N., Farmer, C.B., Hecht, M.H., Bridges, N.T., 2007. Water vapor diffusion in Mars subsurface environments. *Journal of Geophysical Research, Planets* 112, E05016. doi:10.1029/2006JEO02815.
- Kowalewski, D.E., Marchant, D.R., in review. Modeling the effects of thermal contraction-crack polygons on sublimation of buried glacier ice, Antarctica. *Permafrost and Periglacial Processes*.
- Kowalewski, D.E., Marchant, D.R., Levy, J.S., Head, J.W., 2006. Quantifying low rates of summertime sublimation for buried glacier ice in Beacon Valley, Antarctica. *Antarctic Science* 18 (3), 421–428.
- Lambert, F., Delmonte, B., Petit, J.R., Bigler, M., Kaufmann, P.R., Hutterli, M.A., Stocker, T.F., Ruth, U., Steffensen, J.P., Maggi, V., 2008. Dust-climate couplings over the past 800,000 years from the EPICA Dome C ice core. *Nature* 452, 616–619.
- Levy, J.S., Marchant, D.R., Head, J.W., 2006. Distribution and origin of patterned ground on Mullins Valley debris-covered glacier, Antarctica: the roles of ice flow and sublimation. *Antarctic Science* 18 (3), 385–397.
- Lewis, A.R., Marchant, D.R., Ashworth, A.C., Hemming, S.R., Machlus, M.L., 2007. Major middle Miocene global climate change: evidence from East Antarctica and the Transantarctic Mountains. *Geological Society of America Bulletin* 119 (11–12), 1449–1461.
- Linkletter, G., Bockheim, J., Ugolini, F.C., 1973. Soils and glacial deposits in the Beacon Valley, southern Victoria Land, Antarctica. *New Zealand Journal of Geology and Geophysics* 16 (1), 90–108.
- Marchant, D.R., Denton, G.H., 1996. Miocene and Pliocene paleoclimate of the Dry Valleys region, southern Victoria Land: a geomorphological approach. *Marine Micropaleontology* 27 (1–4), 253–271.
- Marchant, D.R., Head, J.W., 2007. Antarctic dry valleys: microclimate zonation, variable geomorphic processes, and implications for assessing climate change on Mars. *Icarus* 192 (1), 187–222.
- Marchant, D.R., Lewis, A.R., Phillips, W.M., Moore, E.J., Souchez, R.A., Denton, G.H., Sugden, D.E., Potter, N., Landis, G.P., 2002. Formation of patterned ground and sublimation till over Miocene glacier ice in Beacon Valley, southern Victoria Land, Antarctica. *Geological Society of America Bulletin* 114 (6), 718–730.
- Marchant, D.R., Phillips, W.M., Schaefer, J.M., Winckler, J.L., Fastook, J.L., Shean, D.E., Kowalewski, D.E., Head, J.W., Lewis, A.R., 2007. Establishing a chronology for the world's oldest glacier ice. In: Cooper, A.K., Raymond, C.R. (Eds.), *International Symposium on Antarctic Earth Sciences*, Santa Barbara, CA. U.S. Geological Survey and The National Academies, Santa Barbara, CA.
- McKay, C., Mellon, M.T., Friedmann, E.I., 1998. Soil temperatures and stability of ice-tempered ground in the McMurdo Dry Valleys, Antarctica. *Antarctic Science* 10 (1), 31–38.
- McKay, C.P., 2009. Snow recurrence sets the depth of dry permafrost at high elevations in the McMurdo Dry Valleys of Antarctica. *Antarctic Science* 21 (1), 89–94.
- Mellon, M.T., Jakosky, B.M., 1993. Geographic variations in the thermal and diffusive stability of ground ice on Mars. *Journal of Geophysical Research, Planets* 98 (E2), 3345–3364. doi:10.1029/92JE02355.
- Mellon, M.T., Jakosky, B.M., 1995. The distribution and behavior of Martian ground ice during past and present epochs. *Journal of Geophysical Research, Planets* 100 (E6), 11781–11799.
- Mellon, M.T., Boynton, W.V., Feldman, W.C., Arvidson, R.E., Titus, T.N., Bandfield, J.L., Putzig, N.E., Sizemore, H.G., 2008. A prelanding assessment of the ice table depth and ground ice characteristics in Martian permafrost at the Phoenix landing site. *Journal of Geophysical Research, Planets* 113 (E00A25).
- Mitrofanov, I., Anfimov, D., Kozyrev, A., Litvak, M., Sanin, A., Tret'yakov, V., Krylov, A., Shvetsov, V., Boynton, W., Shinohara, C., Hamara, D., Saunders, R.S., 2002. Maps of subsurface hydrogen from the high energy neutron detector, Mars Odyssey. *Science* 297 (5578), 78–81.
- Morgan, D., Putkonen, J., Balco, G., Stone, J., 2010. Quantifying regolith erosion rates with cosmogenic nuclides 10Be and 26Al in the McMurdo Dry Valleys, Antarctica. *Journal of Geophysical Research – Earth Surface* 115, 17pp.
- Ng, F., Hallet, B., Sletten, R.S., Stone, J.O., 2005. Fast-growing till over ancient ice in Beacon Valley, Antarctica. *Geology* 33 (2), 121–124.
- Pewe, T.L., 1959. Sand-wedge polygons (tessellations) in the McMurdo Sound region, Antarctica—a progress report. *American Journal of Science* 257, 545–552.
- Plaut, J.J., Safaenili, A., Holt, J.W., Phillips, R.J., Head, J.W., Seu, R., Putzig, N.E., Frigeri, A., 2009. Radar evidence for ice in lobate debris aprons in the mid-northern latitudes of Mars. *Geophysical Research Letters* 36, L02203. doi:10.1029/2008GL036379.
- Rignot, E., Hallet, B., Fountain, A., 2002. Rock glacier surface motion in Beacon Valley, Antarctica, from synthetic-aperture radar interferometry. *Geophysical Research Letters* 29 (12).
- Schaefer, J.M., Baur, H., Denton, G.H., Ivy-Ochs, S., Marchant, D.R., Schluchter, C., Wieler, R., 2000. The oldest ice on Earth in Beacon Valley, Antarctica: new evidence from surface exposure dating. *Earth and Planetary Science Letters* 179 (1), 91–99.

- Schorghofer, N., 2005. A physical mechanism for long-term survival of ground ice in Beacon Valley, Antarctica. *Geophysical Research Letters* 32, L19503. doi:10.1029/2005GL023881.
- Schorghofer, N., 2007. Theory of ground ice stability in sublimation environments. *Physical Review E*. doi:10.1103/PhysRevE.75.041201.
- Schorghofer, N., 2009. Buffering of sublimation loss of subsurface ice by percolating snowmelt: a theoretical analysis. *Permafrost and Periglacial Processes* 20 (3), 309–313.
- Schorghofer, N., Aharonson, O., 2005. Stability and exchange of subsurface ice on Mars. *Journal of Geophysical Research, Planets* 110, E05003. doi:10.1029/2004JE002350.
- Shean, D.E., Marchant, D.R., 2010. Seismic and GPR surveys of Mullins Glacier, McMurdo Dry Valleys, Antarctica: ice thickness, internal structure and implications for surface ridge formation. *Journal of Glaciology* 56 (195), 48–64.
- Shean, D.E., Head, J.W., Marchant, D.R., 2007. Shallow seismic surveys and ice thickness estimates of the Mullins Valley debris-covered glacier, McMurdo Dry Valleys, Antarctica. *Antarctic Science* 19 (4), 485–496.
- Sletten, R.S., Hallet, B., Fletcher, R.C., 2003. Resurfacing time of terrestrial surfaces by the formation and maturation of polygonal patterned ground. *Journal of Geophysical Research, Planets* 108 (8044). doi:10.1029/2002JE001914.
- Stone, J.O., Sletten, R.S., Hallet, B., 2000. Old ice, going fast: cosmogenic isotope measurements on ice beneath the floor of Beacon Valley, Antarctica. *Eos Transactions, American Geophysical Union, Fall Meeting Supplement: Abstract H52C-21*, 81, p. 48.
- Sugden, D.E., Denton, G.H., Marchant, D.R., 1995. Landscape evolution of the Dry Valleys, Transantarctic Mountains - tectonic implications. *Journal of Geophysical Research, Solid Earth* 100 (B6), 9949–9967.
- Vieira, G., Bockheim, J., Guglielmin, M., Balks, M., Abramov, A.A., Boelhouwers, J., Cannone, N., Ganzert, L., Gilichinsky, D.A., Goryachkin, S., Lopez-Martinez, J., Meiklejohn, I., Raffi, R., Ramos, M., Schaefer, C., Serrano, E., Simas, F., Sletten, R., Wagner, D., 2010. Thermal state of permafrost and active-layer monitoring in the Antarctic: advances during the International Polar Year 2007–2009. *Permafrost and Periglacial Processes* 21, 182–197. doi:10.1002/ppp. 685.